Unitary inhibitory field potentials in the CA3 region of rat hippocampus

Michaël Bazelot, Céline Dinocourt, Ivan Cohen and Richard Miles

INSERM U975, CRICM,UPMC, CHU Pitié-Salpêtrière, 105 bd de l'Hôpital, Paris 75013, France

Glickfeld and colleagues (2009) suggested that single hippocampal interneurones generate field potentials at monosynaptic latencies. We pursued this obervation in simultaneous intracellular and multiple extracellular records from the CA3 region of rat hippocampal slices. We confirmed that interneurones evoked field potentials at monosynaptic latencies. Pyramidal cells initiated disynaptic inhibitory field potentials, but did not initiate detectable monosynaptic excitatory fields. We confirmed that inhibitory fields were GABAergic in nature and showed they were suppressed at low external Cl^-, suggesting they originate at postsynaptic sites. Field potentials generated by a single interneurone were detected at multiple sites over distances of more than 800 μm along the stratum pyramidale of the CA3 region. We used arrays of extracellular electrodes to examine amplitude distributions of spontaneous inhibitory fields recorded at sites orthogonal to or along the CA3 stratum pyramidale. Cluster analysis of spatially distributed inhibitory field events let us separate events generated by interneurones terminating on distinct zones of somato-dendritic axis. Events generated at dendritic sites had similar amplitudes but occurred less frequently and had somewhat slower kinetics than perisomatic events generated near the stratum pyramidale. In records from multiple sites in the CA3 stratum pyramidale, we distinguished inhibitory fields that seemed to be initiated by interneurones with spatially distinct axonal arborisations.

(Received 10 December 2009; accepted after revision 15 April 2010; first published online 19 April 2010)
Corresponding author R. Miles: INSERMU975, CHU Pitié-Salpêtrière, 105 bd de l'Hôpital, Paris 75013, France. Email: Richard.Miles@upmc.fr

Introduction

The electroencephalogram and local field potentials are widely used to measure neuronal population activity (Rall & Shepherd, 1968; Niedermeyer & Lopes da Silva, 1999). However neither the components of cellular or synaptic activity that are detected by extracellular fields nor the spatial extent of the populations of elements that generate them are completely clear (Logothetis, 2008). In structures like the hippocampus and cortex, field potentials reflect population EPSPs (Lomo, 1971) resulting from synchronous transmitter release at synapses made onto aligned dendrites of a population of principal cells arranged in a laminar way. Extracellular population EPSPs have been widely used in studies on synaptic function and plasticity (Bliss & Lomo, 1973). Synchronous inhibitory synaptic events also generate field potentials and contribute to the EEG (Haberly & Shepherd, 1973; Pickles & Simmonds, 1978). Simultaneous firing of a neuronal population generates an extracellular population spike (Andersen *et al.* 1971). Slower intrinsic cellular events, such as K^+-mediated afterhyperpolarizations can generate an extracellular field when synchronised in a population of aligned cells (Murakami *et al.* 2002) and simultaneous events in non-neuronal cells can also generate extracellular signals (Dietzel *et al.* 1989).

In all these cases, field potentials reflect transmembrane currents. It is assumed that multiple elements are needed to generate a current that is large and coherent enough to be detected. Elements need to be aligned in space, need to be arranged in an open rather than a closed form and should be synchronously active in time (Rall & Shepherd, 1968; Hubbard *et al.* 1969). Action potentials generated by single neurones can be detected as extracellular spikes, but it has seemed unlikely that a synaptic event initiated by one cell generates a field potential. However recent data suggest that single cells contribute to motor function and sensory perception (Brecht *et al.* 2004; Houweling & Brecht, 2008). In the disinhibited CA3 region, stimulating a single pyramidal cell can generate a field potential with disynaptic latency (Wittner & Miles, 2007) even if it does not initiate firing in a much larger population (Miles & Wong, 1983).

DOI: 10.1113/jphysiol.2009.185918

Glickfeld and colleagues (2009) suggested recently that single hippocampal interneurones of the CA1 region generate small field potentials at monosynaptic latencies. We pursued the circuit origin and the spatial distribution of these signals in the CA3 region of rat hippocampal slices. We confirm that hippocampal inhibitory cells do, and show that pyramidal cells do not, generate detectable monosynaptic fields. In records made from slices in an interface chamber, spontaneous or evoked field potentials generated by interneurones were detected at multiple sites over distances of more than 800 μm along the stratum pyramidale of the CA3 region. Multielectrode records were made to examine the spatial distribution of spontaneous fields along the CA3 stratum pyramidale or along the pyramidal cell somato-dendritic axis. Cluster analysis of spatially distributed inhibitory field events let us separate the activity of interneurones terminating on distinct zones of somato-dendritic membrane or of different interneurones that make spatially distinct perisomatic synapses.

Methods

Slice preparation

Hippocampal slices were prepared from rats of age 7–10 weeks and weight 170–300 g according to the EC Council Directive of November 24, 1986 (86/89/EEC) and INSERM guidelines. Animals were anaesthetised intraperitoneally with ketamine (80 mg kg^{-1}) and xylazine (12 mg kg^{-1}) and perfused intracardially with a solution containing (in mM): sucrose 122, NaCl 62, $NaHCO_3$ 26, KCl 1, $MgCl_2$ 10, $CaCl_2$ 1 and D-glucose 10, equilibrated with 5% CO_2–95% O_2 at 3–5°C. After perfusion, animals were decapitated, both hippocampi were dissected free and transverse slices of thickness 400 μm were cut from the middle third of each hippocampus. Slices were transferred to an interface recording chamber where they were equilibrated with 5% CO_2–95% O_2, heated to 35–37°C and perfused with a solution containing (in mM): NaCl 124, $NaHCO_3$ 26, KCl 3, $MgCl_2$ 2, $CaCl_2$ 2 and glucose 10. In some experiments we examined the effects of a low chloride solution made by reducing the concentration of NaCl to 50 mM with an equimolar substitution of sodium gluconate.

Drugs

$GABA_A$ receptor mediated signalling was suppressed by picrotoxin (50 μM), or bicuculline (20 μM). Fast EPSPs were blocked using 2,3-dihydroxy-6-nitro-7-sulfamoyl-benzo(f)quinoxaline (10 μM, NBQX) and DL-2-amino-5-phosphonovaleric acid (100 μM, DL-APV). Drugs were obtained from Tocris Neuramin (Bioblock, France) or Ascent Scientific (Avonmouth, UK).

Recordings

Extracellular records in some experiments were made with up to four independently positioned electrodes made from tungsten wire of diameter 50 μm and etched to a point (Cohen & Miles, 2000). In other experiments, arrays of eight to ten extracellular recording electrodes were made from nichrome wire of diameter 25 μm (wires from California Fine Wire, Grover Beach, CA, USA). Electrodes were either made in a curved shape so that tips contacted different sites in the CA3 stratum pyramidale or in a linear shape to contact sites orthogonal to the stratum pyramidale along the pyramidal cell somato-dendritic axis. The separation of electrodes in linear arrays was about 100 μm and in arrays to record from the CA3 stratum pyramidale it was 200–300 μm. Electrode arrays were positioned by a manipulator to touch slices in the interface chamber from above. Extracellular signals recorded from independent electrodes were amplified and filtered with a bandpass of 0.1 Hz to 20 kHz (4 channel AM Systems 1700 amplifier, Sequim, WA, USA). Signals from multi-electrode arrays were amplified and filtered with a bandpass of 0.1 Hz to 20 kHz using a custom-made 16 channel amplifier (Dr F. Dubois, Dipsi, Châtillon).

Intracellular records were made with glass electrodes filled with 4 M potassium acetate and bevelled to final resistances of 50–80 MΩ. Signals were amplified in current-clamp mode with an Axoclamp 2B amplifier (Molecular Devices, Sunnyvale, CA, USA) and low-pass filtered at 3 kHz. Intracellular records with overshooting action potentials, an input resistance larger than 20 MΩ and a time constant longer than 10 ms were retained for this study. Biocytin was injected into some neurons so that they could be visualised after recording. Electrodes contained 16 mg ml^{-1} biocytin (Invitrogen, Leek, the Netherlands; in 2 M potassium acetate) which was injected by applying depolarising current steps (200 ms, 1.5 nA at 1 Hz) for 20 min. Slices containing biocytin injected cells were maintained in the recording chamber for 60 min before fixation.

Data treatment

Extracellular and intracellular signals were digitised to a computer with a 12 bit, A–D converter (Digidata 1200A, Molecular Devices) and monitored during experiments with the program Axoscope (Molecular Devices). Signals derived from extracellular recordings were processed (Cohen & Miles, 2000) with routines written in LabView (National Instruments, Austin, TX, USA).

The membrane potential of intracellularly recorded cells was measured if a cell did not fire when no current was injected. Neuronal input resistance and time constant were measured from responses to hyperpolarising current pulses of duration 200 ms and intensity 0.5 nA. We

discriminated between pyramidal cells and interneurones, recorded close to stratum pyramidale, using electrical parameters, including action potential half-width (less than 0.6 ms for interneurones), afterhyperpolarization size and duration (larger than 6 mV and longer than 8 ms for interneurones), time constant (shorter than 15 ms for interneurones and longer for pyramidal cells) as well as dendritic and axonal form after biocytin filled cells were visualized.

Analysis and clustering of extracellular signals

Extracellular action potentials and inhibitory field potentials were detected automatically using a modified version of a previously developed algorithm (Cohen & Miles, 2000). Signals were filtered with a bandpass of 500–3000 Hz for action potentials and 1–300 Hz for field potentials. An 'up-only' transform was then applied together with an adjustable amplitude threshold for event detection. Amplitude was measured from the original signal, and event timing defined from the mid-point of the rising phase. In multi-electrode extracellular records, we detected field potential events that occurred nearly simultaneously across several channels. Events detected on any channel were grouped with events that occurred on any other channel with a delay less than a defined value (2–10 ms) and peak amplitude on each channel was measured.

The amplitudes of signals at different recording sites in multi-channel events could differ suggesting they had distinct origins. We used the standard general mixture model of Gaussian distributions (k-means clustering) to sort multi-channel signals consisting of amplitudes from each electrode, into similar patterns. An expectation-maximization algorithm was used with a relaxed condition on variance of each cluster (Biernacki *et al.* 2006). The Bayesian information criterion (BIC) was used to validate the optimal number of clusters (using software from http://www-math.univ-fcomte.fr/mixmod). Since this procedure tends to minimize the number of clusters, rare events may be included inappropriately. We followed the option in the mixmod software to exclude events (up to 9%) from a cluster if their probability of belonging to it was less than 0.98. We estimated current source density (CSD) from multiple extracellular records regularly spaced along the somato-dendritic axis of CA3 pyramidal cells. The approximation of Nicholson & Freeman(1975) was used for the second spatial derivative of the field potential (bandpass-filtered at 1–300 Hz) with distance:

$$I_x = -\sigma(E_{x-h} - 2E_x + E_{x+h})/4h^2$$

where I_x is current at site x, h is distance between neighbouring electrodes (100 μm in our experiments), E_x is extracellular voltage at site x, E_{x-h} is extracellular voltage at distance $x - h$, E_{x+h} is extracellular voltage at $x + h$, and σ is the tissue conductivity tensor (Taube & Schwartzkroin, 1988). Tissue conductivity varies in anisotropic fashion in different brain regions (Nicholson & Freeman, 1975) and it is therefore difficult to assign a precise value for σ. We chose instead not to include this term in our calculations and expressed the CSD as mV mm^{-2} (Taube & Schwartzkroin, 1988).

Anatomy

We used the lipophilic carbocyanine dye 3,3′-dioctadecyloxacarbocyanine perchlorate (DiO) to mark the position of extracellular electrodes (Matsuo *et al.* 2008). For this purpose, electrodes were dipped into a solution containing DiO dissolved at 10 mg ml^{-1} in dimethyl sulfoxide (DMSO) providing a fluorescent stain of the electrode recording sites in hippocampal slices.

Biocytin was recognised with a fluorescent conjugated streptavidin molecule and neuronal somata were located by immunostaining with an antibody against NeuN.

Slices were fixed overnight in 4% paraformaldehyde in 0.12 M phosphate buffer (PB, pH 7.4), washed in 0.02 M potassium phosphate-buffered saline (KPBS, pH 7.4), and blocked with a solution containing 2% milk powder and 1% Triton X-100 in KPBS for 2 h. Slices were then incubated in a monoclonal mouse antibody against NeuN (1:1000, Chemicon International, Temecula, CA, USA) and Cy3-streptavidin (1/200, Invitrogen) diluted in KPBS with 1% Triton X-100 and 2% milk powder overnight at 4°C. After washing in KPBS, slices were incubated for 4 h in anti-mouse Cy3, to reveal electrode recording sites, or anti-mouse A350, to visualise biocytin-filled interneurones. Slices were then washed and mounted with an antifade reagent (Invitrogen) and coverslipped.

Stacks of images of the CA3 region were acquired with either a ×4 objective of NA 0.16 for NeuN and DiO staining (25–35 images at interval 1 μm with voxel size 1.6 μm), or a ×40 objective of NA 1.3 for biocytin staining (150–300 images at 0.5 μm interval and voxel size 0.16 μm). Reconstructions of biocytin-filled interneurones were realized with Neurolucida (MicroBrightField, Colchester, VT, USA).

Statistics

Values are given as the mean and standard deviation. For statistical analyses Student's t test and a Pearson coefficient for correlation were used (SigmaStat 3.0).

Results

Slow events recorded with extracellular electrodes

In extracellular records from the stratum pyramidale of the CA3 region of hippocampal slices, we detected action potentials and also events with a different form and a slower time course (Fig. 1*A*). Extracellular spikes typically possessed a largely negative waveform of duration 0.7–2.5 ms (Fig. 1*B*). In contrast, distinct spontaneously occurring events possessed a positive waveform with a longer duration of 8–10 ms (Fig. 1*D*). The amplitude of the negative component of extracellular action potentials varied from the noise level of $\sim$8 μV up to 100–150 μV (Fig. 1*C*). The amplitude of the slower, positive extracellular events varied up to about 100 μV (Fig. 1*E*). Slow events occurred at lower frequencies than extracellular action potentials. In 10 records from five slices the mean frequency of slow events was 23.0 ± 10.9 Hz and the mean frequency of extracellular action potentials (of amplitude greater than 10 μV) 52.1 ± 35.2 Hz.

Slow events can be initiated at disynaptic latencies by pyramidal cell firing

Some slow field events were preceded by an extracellular action potential (Fig. 1*A* and *D*) while others seemed to occur independently. In 10 records from five slices, the proportion of slow events following a spike with latency less than 5 ms, varied from 17 to 88%. We therefore asked whether CA3 pyramidal cell firing could initiate slow events. Extracellular responses to single action potentials initiated in pyramidal cells (current injections at 1 Hz, $n = 30$) were examined. Single action potentials in 11 of 30 CA3 pyramidal cells did not evoke slow extracellular events either in single traces or after averaging. In contrast the pyramidal cell shown in Fig. 2*A* often appeared to initiate a slow event in an extracellular record made at a distance of about 100 μm. In this case, the delay between the peak of the intracellular spike and 10% of the maximal amplitude of the extracellular slow event was 2.3 ± 0.7 ms (Fig. 2*Ac*), and the mean amplitude was 49.9 ± 17.3 μV (Fig. 2*Ab*). The mean latency of triggered events from 19 interactions was 2.0 ± 0.6 ms and their mean amplitude was 28.1 ± 9.1 μV. In these interactions a proportion of pyramidal cell action potentials (up to 40%) elicited no extracellular field potential. An example of a pyramidal cell that initiated no extracellular event is shown in Fig. 2*B*. Figure 2*Ca–c* shows a recording where pyramidal cell firing triggered a slow event that was invariably preceded by an extracellular action potential. Such a sequence was evident in five recordings (20%). In this case the mean interval between the intracellular action potential and the slow event was 2.9 ± 1.2 ms and the interval between the extracellular spike and the slow

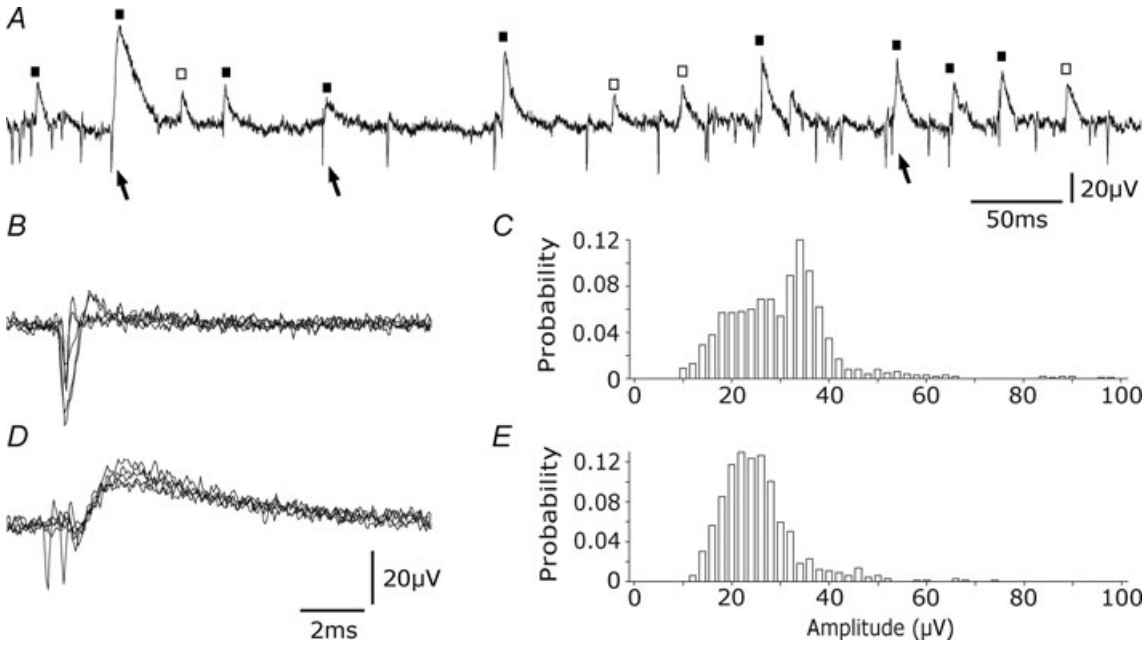

Figure 1. Differences between extracellular slow events and action potentials
A, both action potentials (arrows) and slower extracellular events (squares) are evident in an extracellular recording from the stratum pyramidale of the CA3 region. Slow events were sometimes preceded by action potentials (filled squares) and sometimes not preceded (open squares). *B*, action potentials (5 traces). *C*, amplitude distribution of 200 successive action potentials. *D*, slow extracellular events (5 traces). *E*, amplitude distribution of 200 slow events.

event was 0.6 ± 0.3 ms. Thus some neurones do initiate slow extracellular potentials at monosynaptic latencies.

Slow field events reflect inhibitory signalling

We tested the possibility that interneurones initiate extracellular slow potentials by suppressing GABAergic signalling, by attempting to null the reversal of events mediated by Cl^- and by comparing extracellular events with inhibitory synaptic events recorded from pyramidal cells.

Figure 3 shows that blocking excitatory synaptic transmission with NBQX (10 μM) and APV (100 μM) did not suppress slow events, although it reduced their frequency from 23.0 ± 10.9 Hz to 7.3 ± 6 Hz (10 records from 5 slices, $P < 0.001$). These data suggest that extracellular slow events reflect inhibitory field potentials. If so, they should be nulled near the reversal potential of $GABA_A$ receptor operated channels. We tested this hypothesis by reducing external Cl^- from 150 to 50 mM. Chloride was replaced on an equimolar basis by gluconate. Figure 3*B* and *C* show that slow extracellular events were completely and reversibly suppressed in the low-Cl extracellular solution ($n = 8$). We tested the effects of specific antagonists to confirm that extracellular slow events corresponded to inhibitory synaptic events mediated by $GABA_A$ receptors (Fig. 3*D*) In all cases they were completely suppressed by picrotoxin (50 μM; $n = 3$) or bicuculline (20 μM, $n = 4$).

We next compared the occurrence of slow extracellular events and IPSPs in single pyramidal cells (Fig. 4). Intracellular records were made, in the presence of NBQX and APV to isolate inhibitory signalling, using QX314-containing electrodes so that the amplitude of spontaneous IPSPs could be increased at membrane potentials in the range -30 to -40 mV. The occurrence of slow extracellular events often seemed to be correlated with that of intracellular IPSPs (Fig. 4*A*, $n = 7$). The

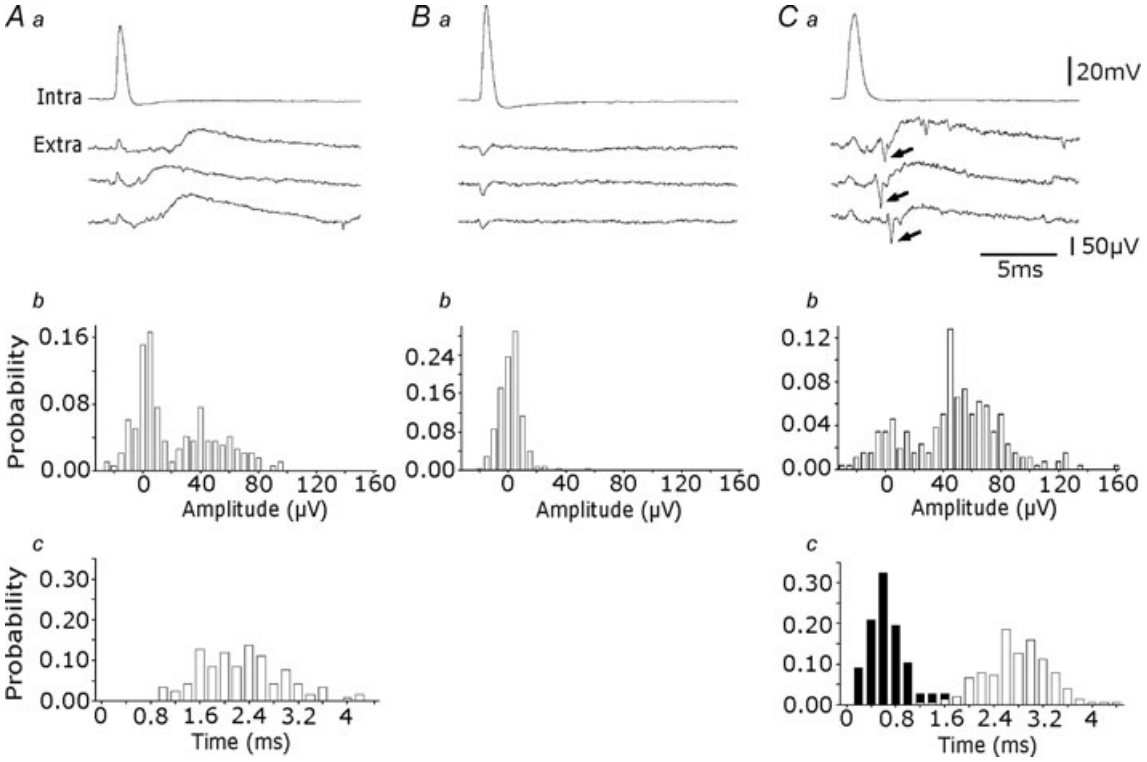

Figure 2. Extracellular events triggered by pyramidal cells
Aa, three slow extracellular events elicited by single action potentials of an intracellularly recorded pyramidal cell. *b*, amplitude distribution of events ($n = 200$), measured to their peak or to the peak of the averaged event for signals smaller than 20 μV. About 70% of pyramidal cell spikes evoked an extracellular signal in this recording. *c*, their latency, from the peak of the intracellular spike to the 10% amplitude of the extracellular event, varied between 1.0 and 4.2 ms. *Ba*, a pyramidal cell that did not evoke an extracellular event. *b*, amplitude distribution of extracellular signals ($n = 200$) measured at 3.5 ms after the peak of the intracellular spike revealed a single peak centred near 0 μV. *Ca*, interactions initiated by a pyramidal cell, where an extracellular spike (arrow) preceeds each slow event. *b*, amplitude distribution of extracellular events measured as in *Ab* ($n = 200$). *c*, distribution of the delays between intracellular spikes and extracellular slow events (white bars; $n = 100$) and between extracellular spikes and slow events (black bars; $n = 100$). Measurements as in *Ac*. The peak latency between the extracellular spike and slow event was 0.6 ms and that between the intracellular spike and the slow event was about 3 ms.

proportion of IPSPs with an onset time within 1 ms of that for an extracellular event varied between 20 and 85% ($n = 7$). Figure 4*B* shows results from a dual recording in which most extracellular field events occurred simultaneously with an intracellular IPSP. A proportion of IPSPs had no extracellular correlate and no intracellular IPSP accompanied some field events.

Figure 4*A* shows inhibitory synaptic events initiated by weak local stimulation in stratum pyramidale were accompanied by an extracellular field (in 10 μM NBQX and 100 μM DL-APV). We compared the kinetics of the fields to those of intracellular IPSPs evoked by the same stimuli and to membrane responses to small, short current injections (Fig. 4*C*). The decay time constant of intracellular IPSPs was 18.9 ± 6.6 ms (Fig. 4*D*), and that of membrane reponses to hyperpolarizations of 3–7 mV amplitude was 16.3 ± 5.2 ms ($n = 7$, Fig. 4*E*). As expected for an extracellular potential due to a transmembrane current (Nicholson & Freeman, 1975), field potentials decayed more quickly than either intracellular event with a mean time constant of 6.9 ± 1.9 ms ($n = 7$, Fig. 4*D*).

Interneurones generate slow field events widely distributed along stratum pyramidale

We next examined extracellular fields initiated by interneurones with somata located close to stratum pyramidale (Fig. 5). Inhibitory cells were recognised by specific firing patterns or by subsequent morphology. Single action potentials in 6 out of 8 interneurones initiated slow field events. The interneurone shown in Fig. 5*A* triggered a slow field event with a mean amplitude of 37.2 ± 21.1 μV (Fig. 5*B*) and a mean delay of 0.7 ± 0.2 ms (Fig. 5*C*). The mean latency of fields triggered in six interactions was 0.6 ± 0.4 ms, and the peak amplitude of averaged fields was 23.4 ± 8.6 μV ($n = 6$). In some records, a proportion of interneurone action potentials appeared not to generate an extracellular field, but records with a better signal to noise ratio are needed to resolve this point.

Field events initiated by a single interneurone could be recorded over a distance of several hundred micrometres along the CA3 stratum pyramidale. Figure 5*D* shows a recording in which inhibitory cell firing initiated field potentials at four sites each separated by about 200 μm. The mean amplitude of evoked field potentials typically decreased with distance from the stimulated cell (Fig. 5*E*). The recording sites in this case are shown stained with DiO in Fig. 5*F*. Figure 5*G* shows the reconstructed axon arborization of a perisomatic targetting biocytin-filled interneurone. Axon terminals (Fig. 5 inset) were distributed in stratum pyramidale over several hundred micrometres from the soma of the recorded cell and their density tended to fall with distance. Intracellular action potentials elicited extracellular field potentials at two of three recording sites in stratum pyramidale (Fig. 5*H* and *Ea–b*). In contrast, no extracellular event was detected by a third electrode located at a site which was not innervated by this cell. The extended spatial distribution of field potentials along the stratum pyramidale is therefore similar to the distribution of terminals of a perisomatic inhibitory interneurone (Gulyás *et al.* 1993; Buhl *et al.* 1994). It is rather larger than that of fields generated by action potentials which fall to noise levels at about 80 μm from the initiating cell (Cohen & Miles, 2000; Henze *et al.* 2000). Inhibitory field distributions appear to be shaped in part by the distribution of terminals made by the cell generating them.

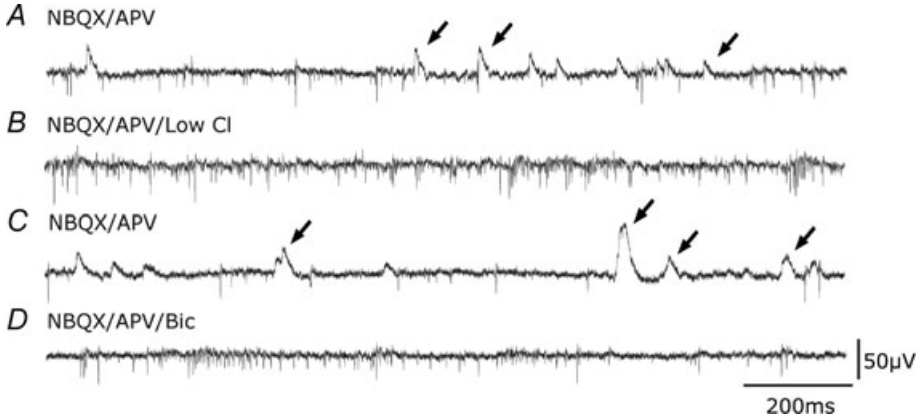

Figure 3. Extracellular events are mediated by $GABA_A$ receptors
A, extracellular traces showing spikes and extracellular field IPSPs (arrows) recorded in the presence of the glutamate-receptor blockers DL-APV (100 μM) and NBQX (10 μM). *B*, slow extracellular events were suppressed when the external concentration of Cl^- was decreased from 130 mM to 50 mM (equimolar replacement by sodium gluconate). Action potential frequency increased. *C*, slow events reappeared on return to the original Cl^- concentration. *D*, the $GABA_A$ receptor antagonist bicuculline (20 μM) suppressed slow extracellular events.

Multi-electrode array records show inhibitory fields have distinct spatial properties

These data suggest that interneurone field potentials extend for considerable distances from the soma that generates them. Extracellular fields generated by different interneurones (Glickfeld *et al.* 2009) might then possess distinct profiles in the somato-dendritic axis of pyramidal cells since different types of interneurone make synapses with distinct membrane regions of all pyramidal cells they innervate (Somogyi *et al.* 1983; Gulyás *et al.* 1993; Buhl *et al.* 1994).

We examined this question in records made with linear arrays of 8–10 electrodes positioned to record along the pyramidal cell somato-dendritic axis and orthogonal to the CA3 stratum pyramidale (Fig. 6*A* and *B*). Spontaneous inhibitory field events were typically recorded by several of these electrodes (Fig. 6*A*). These experiments were done in the presence of NBQX (10 μM) and APV (100 μM) so that different interneurones were not simultaneously excited by a common presynaptic pyramidal cell. Spontaneous field events from multiple electrodes were quantified by detecting field events on any electrode and measuring corresponding potentials at that time on all electrodes (see Methods). In records from six slices, 570–8500 events were measured over periods of 5–20 min (2–7 Hz). K-mean clustering procedures (Fig. 6*C*) were then used to group events with similar spatial profiles of amplitude measured at the different recording sites. Figure 6*D* shows a current source density analysis of field potentials from different

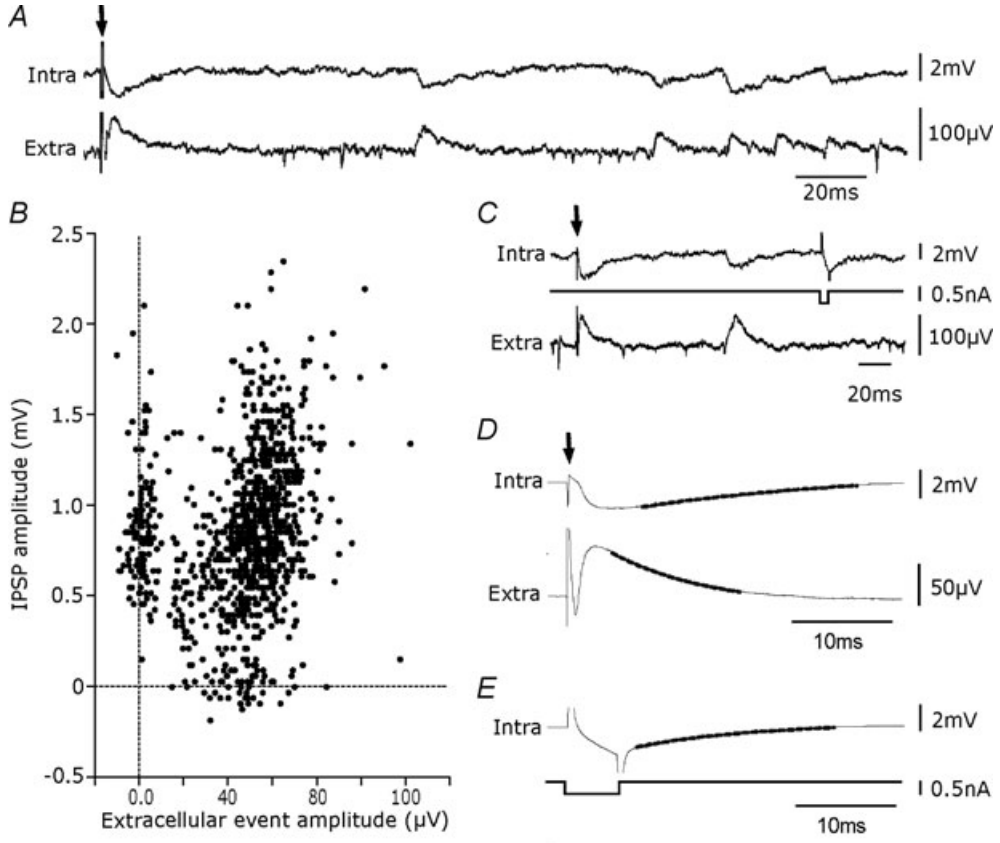

Figure 4. Intracellular correlates of extracellular events
A, intracellular correlates (intra) of extracellular events (extra) occurring spontaneously and elicited by weak local stimulation (stimulation, arrow, in stratum pyramidale at 200 μm from the recorded pyramidal cell, extracellular electrode separated by ~100 μm from the pyramidal cell). Many events were correlated. Records made in the presence of DL-APV (100 μM) and NBQX (10 μM). *B*, amplitude of spontaneous inhibitory field events plotted against that of intracellular IPSPs. Measurements were made to the peak of respective events when either event was detected ($n = 988$). In this recording about 75% ($n = 727$) of intracellular IPSPs were accompanied by an extracellular signal with a difference in onset times of less than 2 ms. Their correlation coefficient, r, was 0.46 ($r^2 = 0.21$, $P < 0.0001$, Pearson). About 9% of extracellular signals were not accompanied by an intracellular IPSP and 16% of IPSPs had no extracellular correlate. *C*, comparison of decay kinetics for the evoked IPSP and response to a small intracellular current injection and the evoked extracellular field. *D*, the intracellular IPSP decayed with a time constant of 23.9 ± 0.1 ms and the field event with a time constant of 9.8 ± 0.4 ms. *E*, the response to a 5 ms hyperpolarizing current step in the same cell decayed with a time constant of 18.3 ± 0.2 ms. Traces in *D* and *E* are averages ($n = 300$) with a mono-exponential fit shown as a thicker line.

clusters which permitted separation of events with a perisomatic or a dendritic source (Nicholson & Freeman, 1975).

In six recordings made with orthogonal arrays, 18 clusters of events were associated with a perisomatic source while 10 others were associated with a dendritic source ($n = 28$ clusters, from 6 multi-electrode records). Figure 7*A* and *B* show examples of these events. There was little difference in the amplitude of field potentials: the mean amplitude of averaged perisomatic events was $19.1 \pm 7.6\,\mu$V and that of dendritic events was $16.2 \pm 8\,\mu$V (Fig. 7*C*, $P = 0.34$, t test). The variability in amplitude of dendritic events was not notably different from that of perisomatic events. The frequency of events

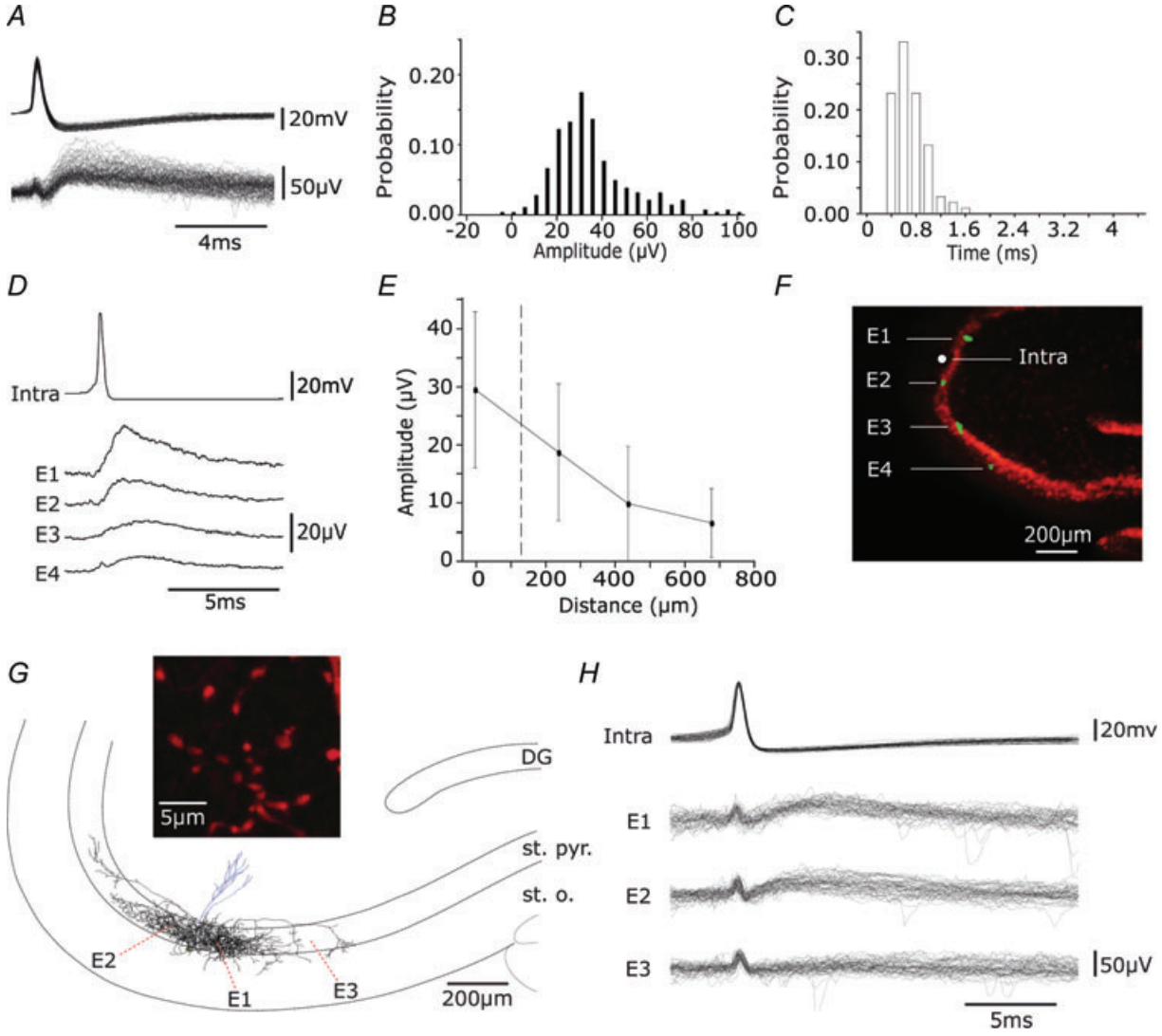

Figure 5. Extracellular events induced by interneurone firing are detected at multiple sites along stratum pyramidale

A, overlay of 100 events elicited by single action potentials of an interneurone. *B*, distribution of amplitudes ($n = 300$). *C*, distribution of latencies ($n = 100$). *D*, averages ($n = 50$) of extracellular events, initiated by single spikes in an interneurone (intra), recorded by 4 extracellular electrodes. Electrodes, E1–E4, were located in CA3 stratum pyramidale at separations of about 200 μm. *E*, mean and standard deviations of the amplitude of extracellular events ($n = 50$) plotted against distance from the recording site. *F*, localization of recording sites with DiO staining. Electrodes were coated with DiO (green) before recording and neuronal somata are shown by immunostaining for NeuN (red). *G*, reconstruction of the dendritic (blue) and axonal (black) arbour of a biocytin-filled perisomatic cell. Axon terminals were largely confined to the CA3 stratum pyramidale (st. pyr.) with some in stratum oriens (st. o.), and were distributed over about 1mm along CA3 st. pyr. The inset shows axon terminals of diameter 1–2 μm. Extracellular records were made from sites E1–3 indicated by red dots. *H*, single action potentials evoked field IPSPs in two of three extracellular records. Thirty responses from electrodes E1–E3 are shown.

with a dendritic source was 0.2 ± 0.1 Hz, rather lower than that of events associated with a somatic source, 2.5 ± 2.2 Hz (Fig. 7*D*, $P < 0.001$, *t* test). We also compared the shape of averaged field potentials at the presumed initiating site for clusters with dendritic sources and those with perisomatic sources. The kinetics of dendritic currents were somewhat slower than those with a perisomatic origin (Banks *et al.* 1998). The mean time to peak for averaged fields corresponding to perisomatic sources was 2.0 ± 0.9 ms while the mean time to peak of dendritic fields was 3.8 ± 1 ms (Fig. 7*E*, $P < 0.0001$, *t* test). The mean decay time constant for perisomatic events was 6.6 ± 1.6 ms while that of dendritic events was 9.6 ± 2.3 ms (Fig. 7*F*, $P < 0.005$, *t* test).

We next attempted to separate the activity of different perisomatic interneurones using electrode arrays to record from multiple sites in CA3 stratum pyramidale. We reasoned that different interneurones may possess distinct axonal arborisations and innervate distinct portions of the CA3 pyramidal layer. If so, comparing amplitudes of spontaneous field events across an array should permit separation of events generated by different interneurones in a similar way to the use of multi-electrode procedures to separate extracellular action potentials (Gray *et al.* 1995).

Records were made with curved arrays consisting of 8–10 electrodes at separation of 200–300 μm to record from multiple sites in the CA3 stratum pyramidale (Fig. 8*A* and *B*). Spontaneous action potentials rarely occurred simultaneously at different sites in multi-electrode records as would be expected from estimates of their spatial extent (Cohen & Miles, 2000; Henze *et al.* 2000). In contrast inhibitory fields of similar shape but usually

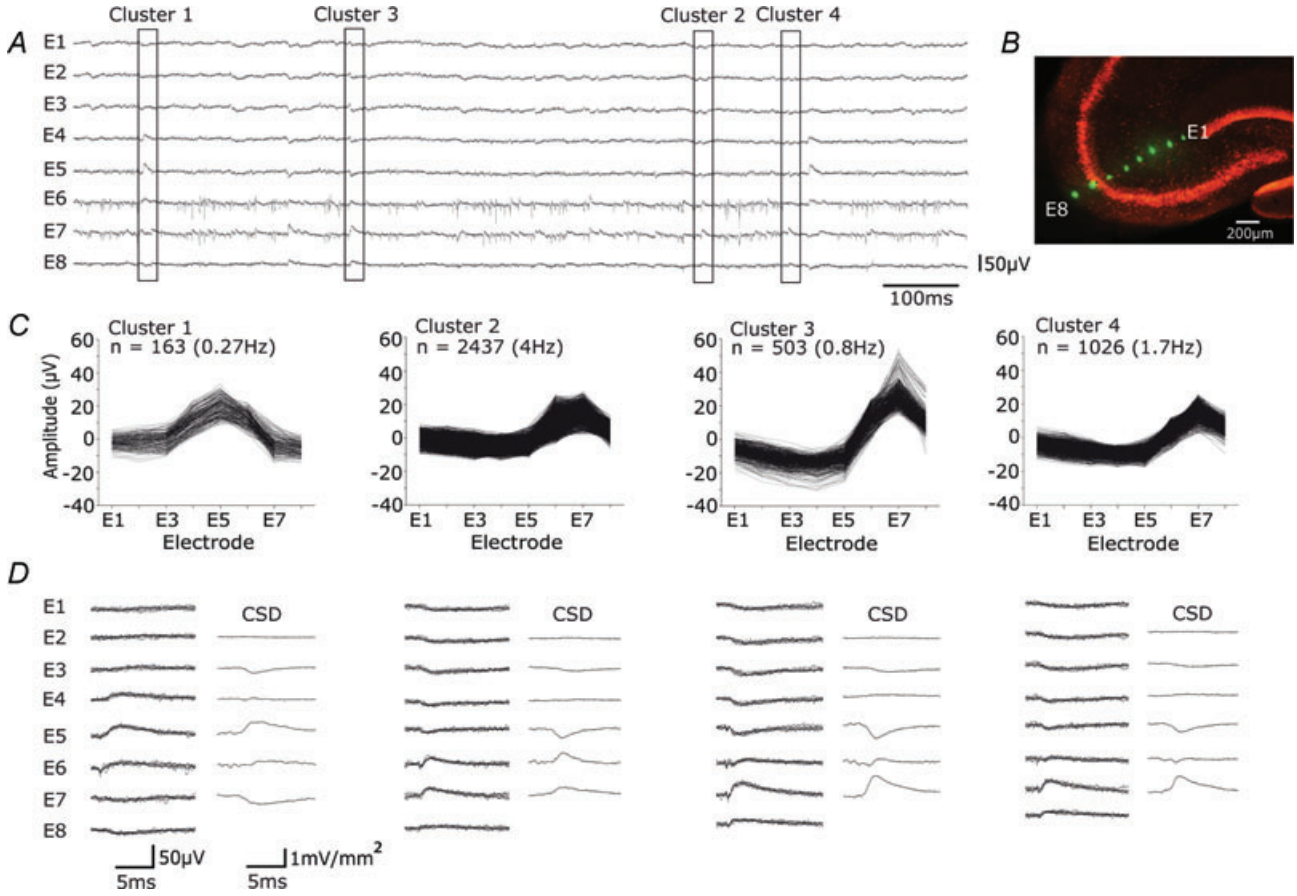

Figure 6. Extracellular signals recorded along the CA3 pyramidal cell somato-dendritic axis
A, spontaneous extracellular signals recorded from multiple sites orthogonal to the CA3 stratum pyramidale with 8 electrodes separated by ~100 μm, in the presence of DL-APV (100 μM) and NBQX (10 μM). Extracellular spikes were limited to electrodes E6 and E7, while field IPSPs were evident in signals from E1–E8. *B*, extracellular recording sites, marked with DiO (green), and neuronal somata by NeuN immunostaining (red). *C* and *D*, K-means cluster analysis separated distinct patterns of signal from the 8 electrodes for 4129 events recorded during 10 min (6.8 Hz). *C*, amplitude distributions for 8 signals and event frequencies from 4 clusters. Cluster 1 corresponds to an infrequent event with maximal amplitude in stratum radiatum, while clusters 2–4 show more frequent events with different distributions and amplitude maxima around stratum pyramidale. *D*, records from each cluster. At left, five superimposed traces from each electrode (E1–E8). At right, current source density analysis as the discrete second spatial derivative of averaged extracellular fields.

different amplitude often occurred nearly simultaneously at multiple sites. Records were made with glutamatergic receptors blocked (NBQX, 10 μM; APV, 100 μM) to prevent simultaneous interneurone firing. Field IPSPs with different spatial profiles were separated by K-means clustering procedures using a BIC to determine the optimal number of clusters. In records from six different slices, 250–3300 events were measured over periods of 5–10 min (0.8–5.5 Hz), and 22 clusters were found. The mean frequency of events from each cluster was 0.7 ± 0.7 Hz and mean maximal field IPSP amplitude was 22.2 ± 7.4 μV. Field IPSPs had a positive amplitude at 1–9 recording sites (mean $= 3.8 \pm 1.6$ sites, $n = 22$) and typically the peak field amplitude of different clusters occurred at distinct sites from CA3a to CA3c. These data suggest that multi-electrode recordings can resolve the activity of multiple simultaneously active interneurones innervating different perisomatic regions of the CA3 pyramidal layer.

Discussion

This work shows that single CA3 interneurones generate field IPSPs (Fig. 2), while single CA3 pyramidal cells do not generate excitatory field events that can be detected. We examined both field IPSPs induced by stimulating single interneurones (Fig. 5) and spontaneously occurring events (Figs 6 and 8). In the CA3 stratum pyramidale, inhibitory fields can be detected over several hundreds of micrometres from the soma of the initiating interneurone suggesting they depend on currents generated simultaneously at many postsynaptic sites. Their amplitude tended to vary reproducibly with distance along the stratum pyramidale. This permitted separation of spontaneous field events with distinct spatial profiles that probably depend on activity in different interneurones (Fig. 8). Multiple field records made from sites orthogonal to stratum pyramidale let us distinguish events initiated at perisomatic or dendritic sites (Fig. 6).

Signal-noise ratio of inhibitory field events

We detected spontaneously occurring extracellular field events of mean amplitude 20–30 μV (Fig. 1*C*). Previous work (Glickfeld *et al.* 2009) resolved averaged field events of amplitude about 15 μV. Several factors could contribute to this difference. First, it might be related to the use of an interface rather than a submerged slice chamber.

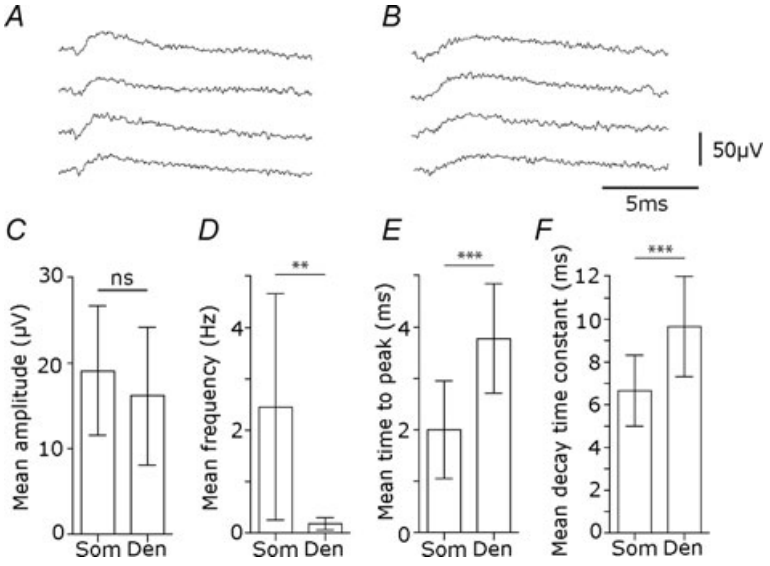

Figure 7. Differences between perisomatic and dendritic inhibitory fields
Dendritic and perisomatically generated fields were separated by current source density analysis of clusters from 6 electrodes. *A*, perisomatic field IPSPs of maximal amplitude in stratum pyramidale. *B*, dendritic field IPSPs of maximal amplitude from an electrode in CA3 stratum radiatum. *C–F*, comparison of amplitude, frequency, time to peak and decay for perisomatic (Som) and dendritic (Den) field events. *C*, the amplitude of perisomatic and dendritic field IPSPs was not different (Som, 19.1 ± 7.6 μV, $n = 18$ clusters; Den, 16.2 ± 8 μV, $n = 10$ clusters; ns, $P = 0.34$, *t* test). *D*, the frequency of events from dendritic field IPSP clusters was lower than that of perisomatic events (Som, 2.45 ± 2.2 Hz, $n = 18$ clusters; Den, 0.17 ± 0.12 Hz, $n = 10$ clusters; $^{**}P < 0.001$, *t* test). *E*, the time to peak, measured from 10 to 90% peak amplitude, was significantly longer for dendritic field IPSPs (Som, 2.0 ± 0.9 ms, $n = 18$ clusters; Den, 3.8 ± 1 ms, $n = 10$ clusters; $^{***}P < 0.0001$, *t* test). *F*, the mean decay time constant (mono-exponential decay fitted to 10–90% amplitude decay for averaged events) was significantly slower for dendritic field IPSPs events (Som, 6.6 ± 1.6 ms, $n = 18$ clusters; Den, 9.6 ± 2.3 ms, $n = 10$ clusters; $^{***}P < 0.0005$, *t* test).

Submerged slices permit visualisation of single neurones, but some properties, including the genesis of population rhythms, may be compromised. Recent work suggests that increasing the effective oxygen tension in a submerged slice increases interneurone activity (Hájos *et al.* 2009; Maier *et al.* 2009). We also used differential amplifiers to acquire field potential signals. Finally different types of electrodes were used. In the Glickfeld study, NaCl-filled glass electrodes of resistance 1–3 MΩ were used, while here we used metal electrodes of resistance of 0.01–0.10 MΩ.

Single interneurones generate a field

Our work began with the observation of extracellular events that did not correspond to action potentials (Fig. 1). These events seem to be generated by GABAergic inhibitory cells. Field events were initiated at monosynaptic latencies by single action potentials in interneurones. They were suppressed by antagonists at $GABA_A$ receptors but not antagonists at glutamate receptors and their amplitude was nulled at reduced external Cl^- concentrations. Extracellular events occurred simultaneously with most but not all intracellularly recorded IPSPs, but decayed more quickly than IPSPs as expected for signals reflecting transmembrane currents.

Field events initiated by a single cell could be recorded over several hundreds of micrometres along the CA3 stratum pyramidale (Fig. 5). Sorting of spontaneous inhibitory field events revealed a similar spatial structure (Fig. 8). In both cases, these spatially distributed field events presumably reflect summed currents generated at postsynaptic sites activated by terminals of a single interneurone. Axons of perisomatic interneurones in the hippocampus extend for several hundreds of micrometres from the soma and form several thousand terminals

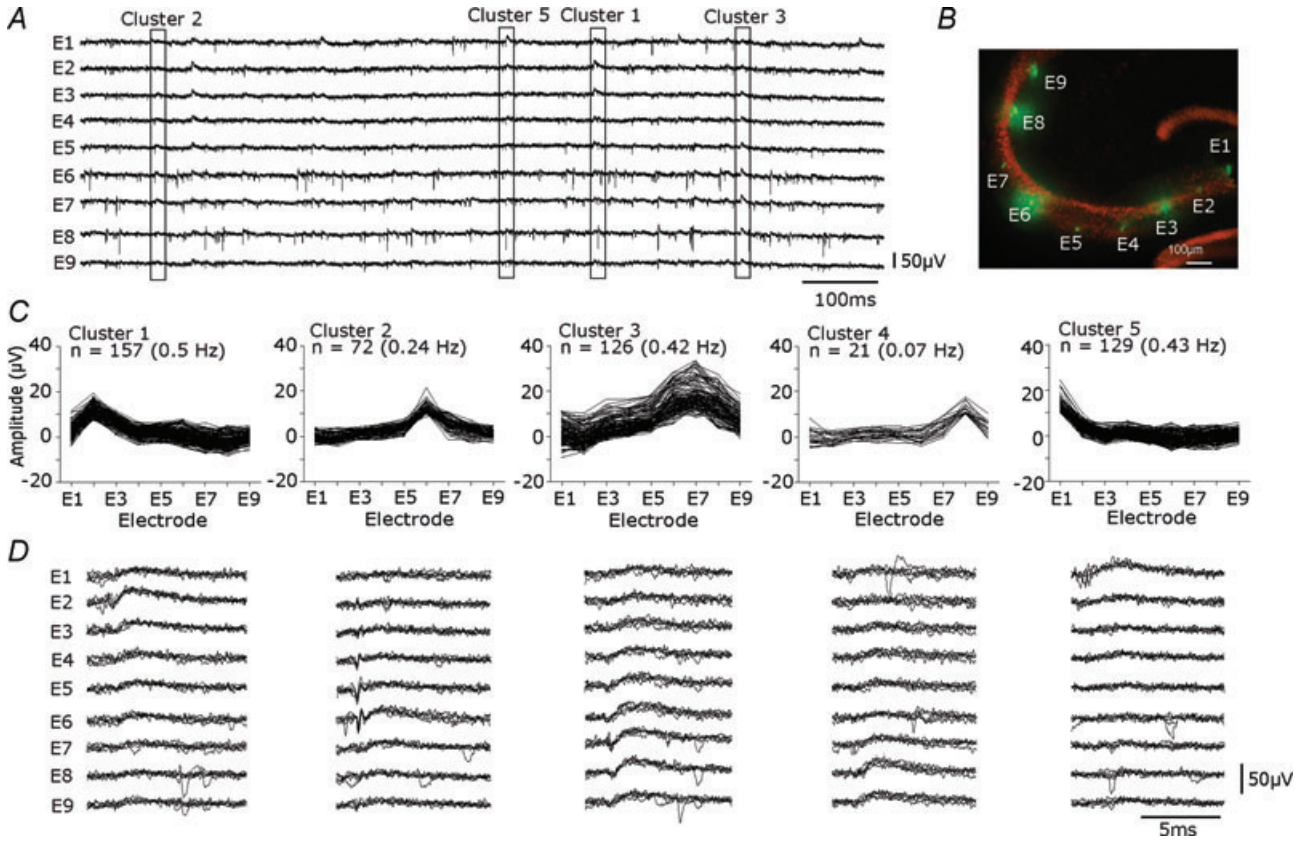

Figure 8. Spontaneous inhibitory field distributions along the CA3 stratum pyramidale
A, extracellular signals recorded from multiple sites of the CA3 stratum pyramidale with 9 extracellular electrodes separated by ∼250 μm. Records made in the presence of DL-APV (100 μM) and NBQX (10 μM). Extracellular spikes, evident on all electrodes, were rarely simultaneous. Field IPSPs, of differing forms and amplitudes were evident at all sites and often occurred simultaneously at several neighbouring electrodes. *B*, location of extracellular recording sites, marked with DiO (green), and neuronal cell bodies detected by NeuN immunostaining for (red). *C* and *D*, K-means cluster analysis was done to separate distinct signal patterns. For 501 events recorded over 5 min, K-means clustering was performed on amplitude values from all electrodes. *C*, shows amplitude distributions from 9 electrodes and the frequencies of events of five clusters in this recording. Each cluster seems to have a distinct at different regions of the CA3 stratum pyramidale. *D*, an overlay of five traces from each electrode (E1–E9) for each cluster.

(Gulyás *et al.* 1993; Buhl *et al.* 1994). Experiments were done in the presence of glutamate receptor antagonists to prevent firing in multiple interneurones innervated by a common pyramidal cell (not shown) which would preclude an accurate determination of distributions of field events generated by single interneurones.

Records from multiple sites showed the variation of sorted, spontaneous fields along the somato-dendritic axis of CA3 pyramidal cells. Current source density analysis indicated a variation in amplitude and polarity along this axis similar to that expected for a single current source and sink in a population of aligned cells (Hubbard *et al.* 1969). We note that certain interneurones, such as bistratified cells (Buhl *et al.* 1996), make terminals at multiple spatially distinct sites and so should generate more complex fields.

Why do single pyramidal cells not generate a field?

Our data suggest that single interneurones do, but single CA3 pyramidal cells do not, generate field potentials. Pyramidal cells did generate inhibitory fields at disynaptic latencies. When several pyramidal cells fire together in disinhibited conditions, negative- rather than positive-going excitatory fields are generated at poly-synaptic latencies (Wittner & Miles, 2007).

The difference in density of GABAergic and glutamatergic terminals probably underlies the generation of unitary inhibitory but not excitatory fields. Single perisomatic interneurones establish several thousand terminals at a density of about 80 per 100 μm^3 (Oláh *et al.* 2009). In contrast, the maximal density of local recurrent terminals made by CA3 pyramidal cells is about 5 per 100 μm^3 (Wittner & Miles, 2007). The amplitude of unitary currents generated at inhibitory and excitatory synaptic sites seems likely to be similar (Jonas *et al.* 1993; Epsztein *et al.* 2006).

Differences between events generated by I-cells contacting P-cells at different sites

Signals recorded from multiple sites along the pyramidal cell somato-dendritic axis (Fig. 6) let us distinguish field potentials with different spatial profiles. Our data suggest that in a slice, interneurones that innervate perisomatic regions of CA3 pyramidal cells were responsible for most spontaneous field events. In the CA1 region, about 40% of inhibitory terminals target CA1 pyramidal cell somata and 33% contact proximal dendrites (Megías *et al.* 2001).

We separated field events with dendritic and perisomatic sources according to amplitude distributions and current source densities. These signals are related to inhibitory currents at the site of generation for many types of interneurones. The decay time of fields derived from dendritic clusters was somewhat slower than that of those associated with perisomatic sources. However the decay of fields with a dendritic source was faster than that reported for some dendritic inhibitory events (Pearce, 1993). Dendritic IPSCs with decay kinetics in the range of tens of milliseconds may result from a slower diffusion of neurotransmitter to postsynaptic receptors (Szabadics *et al.* 2007), or from the expression of $GABA_A$ receptor subunits with slower kinetics (Zarnowska *et al.* 2009). The spontaneously occurring dendritic events we recorded were less frequent than perisomatic events. We did observe some large events with still slower kinetics (Williams *et al.* 1994; Tamás *et al.* 2003), but they were too infrequent (less than 0.05 Hz compared with 0.17 for dendritic events) to be adequately separated by the clustering procedure.

Axo-axonal interneurones initiate depolarizing synaptic events in cortical pyramidal cells (Szabadics *et al.* 2006) and their axon initial segments are depolarized by focal uncaging of GABA (Khirug *et al.* 2008). Depolarizing GABAergic events at axo-axonic terminals made on CA3 pyramidal cells should generate a negative field near the border of stratum pyramidale and stratum oriens, and a positive field in stratum radiatum (Niedermeyer & Lopes da Silva, 1999). Glickfeld and colleagues (2009) found no evidence that axo-axonic cells of the CA1 region generated inhibitory field events of this form. Our data are less direct since they derive from sorted, spontaneous field potentials (Fig. 6*C* and *D*) but also provide no evidence for such a distribution. Possibly the mean relation between membrane potential and IPSP reversal across the population of synaptic sites involving CA3 axo-axonic terminals does not generate field potentials expected for a GABAergic depolarization. Furthermore, numbers of axo-axonic contacts are less than perisomatic inhibitory synaptic contacts (Megías *et al.* 2001).

Conclusion

Action potentials in single CA3 interneurones, but not pyramidal cells, generate spatially distributed field potentials. The difference probably results from the higher local density of terminals established by some interneurones. At moderate levels of pyramidal cell synchrony, these inhibitory signals seem likely not only to control population oscillations (Whittington & Traub, 2003; Mann & Paulsen, 2007) but also to dominate the EEG signals that they generate (Trevelyan, 2009).

References

Andersen P, Bliss TV & Skrede KK (1971). Unit analysis of hippocampal population spikes. *Exp Brain Res* **13**, 208–221.

Banks MI, Li TB & Pearce RA (1998). The synaptic basis of $GABA_{A,slow}$. *J Neurosci* **18**, 1305–1317.

Bliss TV & Lomo T (1973). Long-lasting potentiation of synaptic transmission in the dentate area of the anaesthetized rabbit following stimulation of the perforant path. *J Physiol* **232**, 331–335.

Brecht M, Schneider M, Sakmann B & Margrie TW (2004). Whisker movements evoked by stimulation of single pyramidal cells in rat motor cortex. *Nature* **427**, 704–710.

Biernacki C, Celeux G, Govaert G, Langrognet F (2006). Model-based cluster and discriminant analysis with the MIXMOD software. *Comput Stat Data Anal* **51/2**, 587–600.

Buhl EH, Halasy K & Somogyi P (1994). Diverse sources of hippocampal unitary inhibitory postsynaptic potentials and the number of synaptic release sites. *Nature* **368**, 823–828.

Buhl EH, Szilágyi T, Halasy K & Somogyi P (1996). Physiological properties of anatomically identified basket and bistratified cells in the CA1 area of the rat hippocampus in vitro. *Hippocampus* **6**, 294–305.

Cohen I & Miles R (2000). Contributions of intrinsic and synaptic activities to the generation of neuronal discharges in *in vitro* hippocampus. *J Physiol* **524**, 485–502.

Dietzel I, Heinemann U & Lux HD (1989). Relations between slow extracellular potential changes, glial potassium buffering, and electrolyte and cellular volume changes during neuronal hyperactivity in cat brain. *Glia* **2**, 25–44.

Epsztein J, Milh M, Bihi RI, Jorquera I, Ben-Ari Y, Represa A & Crépel V (2006). Ongoing epileptiform activity in the post-ischemic hippocampus is associated with a permanent shift of the excitatory-inhibitory synaptic balance in CA3 pyramidal neurons. *J Neurosci* **26**, 7082–7092.

Glickfeld LL, Roberts JD, Somogyi P & Scanziani M (2009). Interneurons hyperpolarize pyramidal cells along their entire somatodendritic axis. *Nat Neurosci* **12**, 21–23.

Gray CM, Maldonado PE, Wilson M & McNaughton B (1995). Tetrodes markedly improve the reliability and yield of multiple single-unit isolation from multi-unit recordings in cat striate cortex. *J Neurosci Methods* **63**, 43–54.

Gulyás AI, Miles R, Hájos N & Freund TF (1993). Precision and variability in postsynaptic target selection of inhibitory cells in the hippocampal CA3 region. *Eur J Neurosci* **5**, 1729–1751.

Haberly LB & Shepherd GM (1973). Current-density analysis of summed evoked potentials in opossum prepyriform cortex. *J Neurophysiol* **36**, 789–802.

Hájos N, Ellender TJ, Zemankovics R, Mann EO, Exley R, Cragg SJ, Freund TF & Paulsen O (2009). Maintaining network activity in submerged hippocampal slices: importance of oxygen supply. *Eur J Neurosci* **29**, 319–327.

Henze DA, Borhegyi Z, Csicsvari J, Mamiya A, Harris KD & Buzsáki G (2000). Intracellular features predicted by extracellular recordings in the hippocampus in vivo. *J Neurophysiol* **84**, 390–400.

Houweling AR & Brecht M (2008). Behavioural report of single neuron stimulation in somatosensory cortex. *Nature* **451**, 65–68.

Hubbard JI, Llinas R & Quastel DMJ (1969). *Electrophysiological Analysis of Synaptic Transmission*. E. Arnold, London.

Jonas P, Major G & Sakmann B (1993). Quantal components of unitary EPSCs at the mossy fibre synapse on CA3 pyramidal cells of rat hippocampus. *J Physiol* **472**, 615–663.

Khirug S, Yamada J, Afzalov R, Voipio J, Khiroug L & Kaila K (2008). GABAergic depolarization of the axon initial segment in cortical principal neurons is caused by the Na-K-2Cl cotransporter NKCC1. *J Neurosci* **28**, 4635–4639.

Logothetis NK (2008). What we can do and what we cannot do with fMRI. *Nature* **453**, Supplementary notes 8–13.

Lomo T (1971). Patterns of activation in a monosynaptic cortical pathway: the perforant path input to the dentate area of the hippocampal formation. *Exp Brain Res* **12**, 18–45.

Maier N, Morris G, Johenning FW & Schmitz D (2009). An approach for reliably investigating hippocampal sharp wave-ripples in vitro. *PLoS One* **4**, e6925.

Mann EO & Paulsen O (2007). Role of GABAergic inhibition in hippocampal network oscillations. *Trends Neurosci* **30**, 343–349.

Matsuo N, Reijmers L & Mayford M (2008). Spine-type-specific recruitment of newly synthesized AMPA receptors with learning. *Science* **319**, 1104–1107.

Megías M, Emri Z, Freund TF & Gulyás AI (2001). Total number and distribution of inhibitory and excitatory synapses on hippocampal CA1 pyramidal cells. *Neuroscience* **102**, 527–540.

Miles R & Wong RKS (1983). Single neurones can initiate synchronised population discharges in the hippocampus. *Nature* **306**, 371–374.

Murakami S, Zhang T, Hirose A & Okada YC (2002). Physiological origins of evoked magnetic fields and extracellular field potentials produced by guinea-pig CA3 hippocampal slices. *J Physiol* **544**, 237–251.

Nicholson C & Freeman JA (1975). Theory of current source-density analysis and determination of conductivity tensor for anuran cerebellum. *J Neurophysiol* **38**, 356–368.

Niedermeyer E & Lopes da Silva FH (1999). Biophysical aspects of EEG and magnetoencephalogram generation. In *Electroencephalography: Basic Principles, Clinical Applications and Related Fields*, 4th edn, ed. Keating M, Magee RD & Mitchell C, pp. 93–109. Williams and Wilkins, Baltimore.

Oláh S, Füle M, Komlósi G, Varga C, Báldi R, Barzó P & Tamás G (2009). Regulation of cortical microcircuits by unitary GABA-mediated volume transmission. *Nature* **461**, 1278–1281.

Pearce RA (1993). Physiological evidence for two distinct $GABA_A$ responses in rat hippocampus. *Neuron* **10**, 189–200.

Pickles HG & Simmonds MA (1978). Field potentials, inhibition and the effect of pentobarbitone in the rat olfactory cortex slice. *J Physiol* **275**, 135–148.

Rall W & Shepherd GM (1968). Theoretical reconstruction of field potentials and dendrodendritic synaptic interactions in olfactory bulb. *J Neurophysiol* **31**, 884–915.

Somogyi P, Nunzi MG, Gorio A & Smith AD (1983). A new type of specific interneuron in the monkey hippocampus forming synapses exclusively with the axon initial segments of pyramidal cells. *Brain Res* **259**, 137–142.

Szabadics J, Varga C, Molnar G, Olah S, Barzo P, Tamás G (2006). Excitatory effect of GABAergic axo-axonic cells in cortical microcircuits. *Science* **311**, 233–235.

Szabadics J, Tamás G & Soltesz I (2007). Different transmitter transients underlie presynaptic cell type specificity of $GABA_A$,slow and $GABA_A$,fast. *Proc Natl Acad Sci U S A* **104**, 14831–14836.

Tamás G, Lorincz A, Simon A & Szabadics J (2003). Identified sources and targets of slow inhibition in the neocortex. *Science* **299**, 1902–1905.

Taube JS & Schwartzkroin PA (1988). Mechanisms of long-term potentiation: a current-source density analysis. *J Neurosci* **8**, 1645–1655.

Trevelyan AJ (2009). The direct relationship between inhibitory currents and local field potentials. *J Neurosci* **29**, 15299–15307.

Whittington MA & Traub RD (2003). Inhibitory interneurons and network oscillations in vitro. *Trends Neurosci* **26**, 676–682.

Williams S, Samulack DD, Beaulieu C & LaCaille JC (1994). Membrane properties and synaptic responses of interneurons located near the stratum lacunosum-moleculare/radiatum border of area CA1 in whole-cell recordings from rat hippocampal slices. *J Neurophysiol* **71**, 2217–2235.

Wittner L & Miles R (2007). Factors defining a pacemaker region for synchrony in the hippocampus. *J Physiol* **584**, 867–883.

Zarnowska ED, Keist R, Rudolph U & Pearce RA (2009). $GABA_A$ receptor $\alpha 5$ subunits contribute to $GABA_{A,slow}$ synaptic inhibition in mouse hippocampus. *J Neurophysiol* **101**, 1179–1191.

Author contributions

This work was performed at the CHU Pitié-Salpêtrière. All authors contributed to the design of experiments. M.B. performed most of the recording and data analysis. R.M. did much of the writing with M.B., C.D. and I.C. I.C. contributed to amplifier design and data analysis and C.D. to anatomical work. All authors approved the final version of the manuscript.

Acknowledgements

We thank Attila Gulyás for comments. We gratefully acknowledge financial support from INSERM, UPMC, FRM, ANR (08MNP006), and the NIH (MH054671).